Incorporating Multiscale Micromechanical Approach into PLSNs with Different Intercalated Morphologies

A. Zehtab Yazdi, R. Bagheri, M. Kazeminezhad, D. Heidarian

Polymeric Materials Research Group, Department of Materials Science and Engineering, Sharif University of Technology, Tehran, Iran

Received 7 January 2010; accepted 12 June 2010
DOI 10.1002/app.33011
Published online 29 September 2010 in Wiley Online Library (wileyonlinelibrary.com).

ABSTRACT: The objective of the present study is to predict Young's modulus of polymer-layered silicate nanocomposites (PLSNs) containing fully intercalated structures. The particular contribution of this article is to consider the changes in structural parameters of different intercalated morphologies in vicinity of each other. These parameters include aspect ratio of intercalated stacks, number of silicate layers per stack, *d*-spacing between the layers, modulus of the gallery phase, and volume fraction of each intercalated morphology. To do this, the effective particle concept has been employed and combined with the Mori-Tanaka micromechanical model. It has been shown that the simultaneous effects of *d*-spacing between the silicate layers and gallery phase modulus remarkably influence the nanocomposite's modulus. Finally, the micromechanical modeling results have been compared with the experimental data and illustrates that the new approach is more accurate than the earlier model developed by the same authors. © 2010 Wiley Periodicals, Inc. J Appl Polym Sci 119: 3347–3359, 2011

Key words: polymer layered silicate nanocomposites (PLSNs); multiscale micromechanical modeling; fully intercalated structures

INTRODUCTION

Outstanding mechanical properties,[1,2] reduced flammability,[3,4] and gas permeability[5,6] of the polymer layered silicate nanocomposites (PLSNs) have attracted investigators in recent years. The enhancements are function of the large aspect ratio and large surface area of the clay mineral, the strong interactions between the polymer chains and the layered silicate, and the nano-scale structure of the polymer nanocomposite.[7]

The morphology of PLSNs has a hierarchical structure demonstrating nano-, meso-, and micro-level morphologies in the vicinity of each other. The clay dispersion in the matrix is typically described in terms of intercalation versus exfoliation. In the intercalated structure, polymer chains enter into the gallery spacing between the clay platelets and expanded them to a typical interlayer spacing of the order of 1–4 nm. This spacing can be measured by X-ray diffraction method. In the exfoliated nanostructure, the clay platelets are individually dispersed in the polymer matrix and optimal interaction between the clay and polymer occurs.[8] However, the structural parameters affecting the mechanical properties of PLSNs containing intercalated structures are much more than those with exfoliated structures.[9] These parameters are listed below and some of them have been experimentally investigated by the researchers[10–17]:

- exfoliated/intercalated ratio,[10–13]
- aspect ratio of both clay platelets and stacks,[14,15]
- silicate layer spacing (*d*-spacing),[16]
- number of the silicate layers per stack, and
- properties of the gallery phase between the silicate layers.

Although there have been numerous material syntheses, tests and characterizations of PLSNs with fully intercalated structures, the fundamental mechanisms for mechanical properties enhancement are not fully understood and are rarely discussed.[17–20] Therefore, conducting some qualitative and quantitative analysis to predict the stiffening effect of the silicate nanolayers would accelerate the development of such nanocomposites. Among different models proposed in this area, several micromechanical approaches[21–30] in particular to those which are based on the Mori-Tanaka model[31] are mostly considered and developed. The Mori-Tanaka model has proven to be quite accurate in predicting the effective mechanical properties of various composites with either random orientation or total alignment of the reinforcements.[32] However, only a few researches[24,25] based on the

Correspondence to: R. Bagheri (rezabagh@sharif.edu).

Mori-Tanaka theory have investigated the complex effects of such structural parameters in PLSNs with fully intercalated structures.

Figiel and Buckly[21] in their recent study employed the concept of the effective particle in calculating the elastic constants with two continuum approaches including the FEM-based numerical analysis and the Mori-Tanaka theory. They found that the effective particle approach was a useful and accurate means of homogenizing the stacks of platelets in a nanocomposite with intercalated morphology. Luo and Daniel[24] applied the Mori-Tanaka model to predict the modulus of PLSNs as a function of structural parameters. Besides, Sheng et al.[25] predicted the overall elastic modulus of the amorphous and semicrystalline polymer clay nanocomposites and their dependence on the matrix and clay properties as well as internal clay structural parameters.

However, there seems to be some major deficiencies in the research studies mentioned above.[21,24,25] New TEM studies[17] illustrated that in some cases, different intercalated morphologies can be present in a single polymer matrix, the point which has not been regarded before. Besides, Adame and Beall[33] based on the AFM observations showed that the gallery phase between the silicate layers in the intercalated structures has a main contribution on the properties of PLSNs.

Considering above deficiencies, the authors in their previous work[34] proposed an approach based on the Halpin-Tsai model and the effective particle concept to predict the modulus of PLSNs with different intercalated morphologies. Although this approach considered most of the structural parameters which had not been reported before and fitted some of the experimental data in a satisfactory way, it could not predict very well some of the experiments, especially those which are concerning the *d*-spacing variations between the silicate layers. This might be firstly due to the fact that reinforcements in the Halpin-Tsai model have unidirectional orientations within the matrix. Besides, the model is not as accurate as the Mori-Tanaka model to predict Young's modulus of the composites containing fillers with large aspect ratio.[32] Therefore, the authors in their present study employed the Mori-Tanaka model in estimating the nanocomposite's modulus with different intercalated morphologies. Correspondingly, the new model considers various structural parameters including *d*-spacing between the silicate layers, the number of silicate sheets per stack, the contributions of the gallery phase in each cluster and aspect ratio of the intercalated stack. Because the multi-scale micromechanical model based on the Mori-Tanaka can consider a more complex shape of reinforcements, it shows better agreement with the experimental data than the previous approach proposed by the authors.[34]

PLSNs containing fully intercalated structure

Because most of PLSNs demonstrate partially or fully intercalated structure, nowadays, extensive studies have been conducted either experimentally[10–16] or theoretically[24,25,34] to investigate the effects of nanostructural parameters on Young's modulus of the nanocomposites. Penetration of polymer chains along silicate layers is the most characteristic of those structures which consequently composes the so-called "gallery phase" (Fig. 1). This phase is consisted of polymer chains and chemical compounds added during various stages of synthesis and processing. Up to now, it is speculated that intercalated stacks are homogeneously distributed through the polymer matrix,[24,25] however, in some cases different intercalated morphologies can be characterized (Fig. 2). These differences are mostly due to the number of silicate layers per stack (N), d-spacing between the layers (d_{001}) and gallery phase modulus (E_g). The main purpose of this research is to propose a multi-scale micromechanical approach based on the Mori-Tanaka model that considers different intercalated morphologies in the vicinity of each other. However, there is no report in the literature investigating micromechanically these complex hierarchical structures.

Micromechanical approach

Here, Young's modulus of polymer layered silicate nanocomposites with fully intercalated structures, as described in previous section, is predicted. After providing a good background for the Mori-Tanaka model in Background section, the effective particle concept in Model development section is employed in estimating the nanostructural characteristics of different intercalated morphologies in vicinity of each other. Then, these two models are combined and the stiffness tensor of such nanocomposite is predicted as a function of structural characteristics.

Background

The effective stiffness tensor (C) of the composite can be expressed by using the Mori-Tanaka method[31] adapted by Benveniste[37,38] as:

$$C = C_1 + \sum_{r=2}^{N} c_r\{(C_r - C_1)T_r\}\left[\sum_{r=1}^{N} c_r\{T_r\}\right]^{-1} \quad (1)$$

where the capital letters represent tensors. The composite is consisted of ($N-1$) kinds of discrete inclusions ($r = 2,\ldots, N$) that can be different in stiffness and/or shape. The volume fraction of the r-th phase is denoted by (c_r). In the present article, we always assume that the continuous matrix is an isotropic material which simulates a polymer. The tensor T_r, namely, the so-called Wu's tensor,[39] in eq. (1) is:

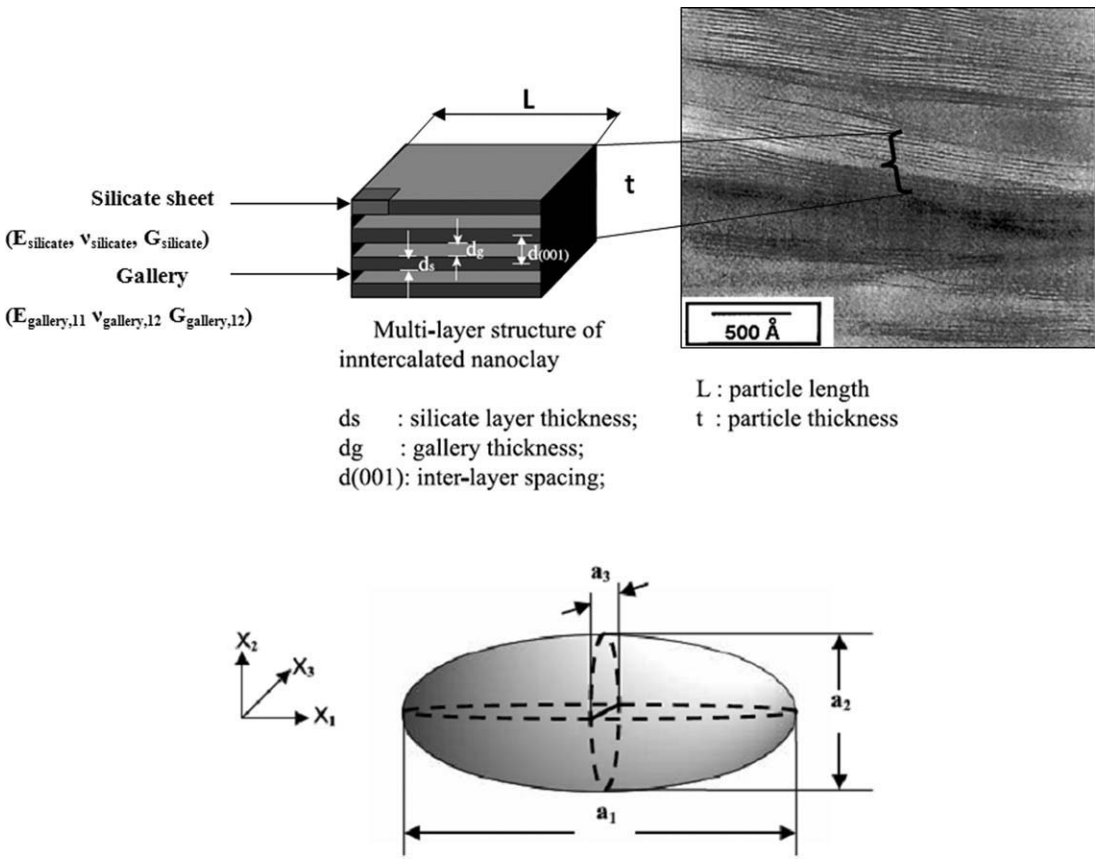

Figure 1 (a) TEM image of poly styrene-3 wt % clay nanocomposite together with schematic illustration of intercalated structure. (b) Schematic illustration of a three dimensional ellipsoidal inclusion, characterized by two aspect ratios. A primary aspect ratio $\alpha = a_1/a_3$ and a secondary aspect ratio $\beta = a_1/a_2$.[41] (Adapted from Ref. 35).

$$T_r = [I + S_r C_1^{-1}(C_r - C_1)]^{-1} \quad (2)$$

where S_r is the Eshelby's transformation tensor[40] corresponding to the r-th phase that can be found in the Ref. 41 as shown in Appendix. I_r is the fourth-order symmetric unit tensor. Curly brackets {} in eq. (1) represent an average over all possible orientations. When the orientation of each inclusion is described using the Euler angles (Fig. 3), the orientation-dependent part can be expressed as:

$$C_{ijkl} = a_{ip}a_{jq}a_{kr}a_{ls}C_{pqrs} \quad (3)$$

where the components of a_{ij} (ϕ, ψ, θ) can be written as:

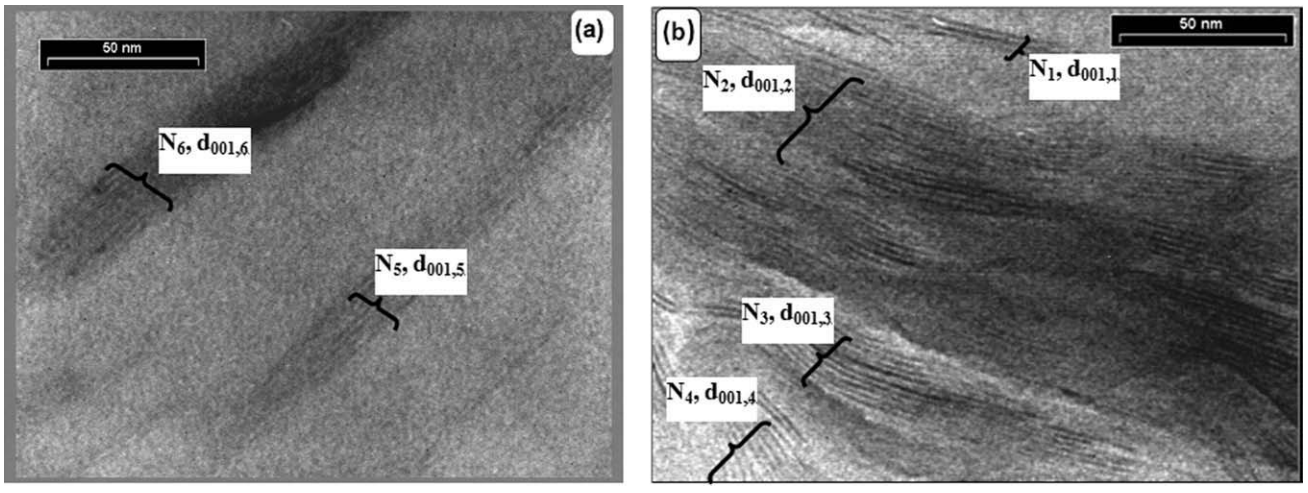

Figure 2 TEM images of (a) Epoxy-5 wt %[36] and (b) Epoxy-3 wt %[17] clay nanocomposites containing six different intercalated morphologies.

$$[a_{ij}] = \begin{bmatrix} \cos\theta\cos\varphi\cos\psi - \sin\varphi\sin\psi & \cos\theta\sin\varphi\cos\psi - \cos\varphi\sin\psi & -\sin\theta\cos\psi \\ -\cos\theta\cos\varphi\sin\psi - \sin\varphi\cos\psi & -\cos\theta\cos\varphi\sin\psi - \cos\varphi\cos\psi & \sin\theta\sin\psi \\ \sin\theta\cos\varphi & \sin\theta\sin\varphi & \cos\theta \end{bmatrix} \quad (4)$$

The orientation average then follows from:

$$\{C\} = \int_0^{2\pi}\int_0^{2\pi}\int_0^{\pi} C_{ijkl}(\theta,\varphi,\psi) \times f(\theta,\varphi,\psi) \times \sin(\theta) d\theta d\varphi d\psi \quad (5)$$

where f (ϕ, ψ, θ) is the orientation distribution function defined in the Euler coordinates (ϕ, ψ, θ). Finally, the effective Young's modulus (E) of the composite is obtained through the following relation:

$$E = C_{11} - \frac{C_{12}^2}{C_{11} + C_{12}} \quad (6)$$

Model development

To obtain the effective stiffness tensor of such nanocomposites, a representative volume element (RVE) according to the heterogeneous intercalated structure is needed. The RVE should be the smallest possible unit which includes all distinct parameters of the hierarchical structure, as shown in Figure 4. In the real cases, there are different intercalated morphologies within a polymer matrix, as shown in Figure 2. However, to avoid being confused the sensitivity analysis in Numerical Results and Discussion section, the RVE in this article is consisted of only two various intercalated morphologies. These morphologies are quite different from each others from aspect ratio, d-spacing, gallery phase modulus, and number of silicate layers points of view.

Accordingly, the three phase form of the Mori-Tanaka model has been employed as follows:

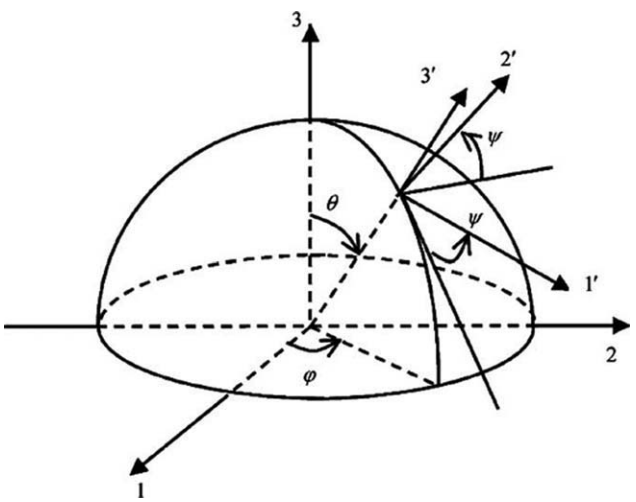

Figure 3 Euler angles defining the relation between the local coordinate system (1′2′3′) and the global coordinate system (123).[41]

$$C = C_1 + [c_2\{(C_2 - C_1)T_2\} + c_3\{(C_3 - C_1)T_3\}][c_1 I + c_2\{T_2\} + c_3\{T_3\}]^{-1} \quad (7)$$

where the corresponding Wu's tensor can be written as:

$$T_3 = [I + S_3 C_1^{-1}(C_3 - C_1)]^{-1} \quad (8)$$

$$T_2 = [I + S_2 C_1^{-1}(C_2 - C_1)]^{-1} \quad (9)$$

In eqs. (7)–(9), the subscripts 1–3 denote the polymer matrix, intercalated morphology 1 and intercalated morphology 2, respectively.

Basically, the Mori-Tanaka model [eqs. (7)–(9)] is consisted of four significant elements, including stiffness tensor (C_i), Eshelby's tensor (S_i), average over all possible directions {}, and volume fraction (c_i), as shown in Figure 5.

As seen in Figure 5, to compute each part of eqs. (7)–(9), it is needed to correlate the properties of each phase (i.e., Young's modulus, Poisson's ratio, aspect ratio) with the nanostructural parameters (i.e., number of silicate layers per stack, d-spacing between the silicate layers and gallery phase between the layers). To do this, researchers[18,25] based on the experimental observations proposed a practical model called "effective particle concept" considering homogeneous intercalated structures. However, recent experimental studies[33] have shown that in some circumstances, different intercalated morphologies can be obtained in a single polymer matrix. Therefore, the effective particle concept should be developed so as to consider a variety of intercalated morphologies with different volume fractions and properties. The precise contribution of this article is to develop the concept for two different intercalated morphologies and considers the effect of gallery phase on Young's modulus of PLSNs.

For simplicity, the internal structure of an intercalated clay particle is idealized as a multi-layer stack containing N single silicate sheets with an effective thickness (d_s) and uniform interlayer spacing (d_{001}), as shown in Figure 1. The particle thickness (t) can be related to the internal structural parameters N and d_{001} through:

$$t = (N - 1)d_{001} + d_s \quad (10)$$

The important parameter of the clay particle structure is the number of silicate sheets per unit particle thickness (X_N):

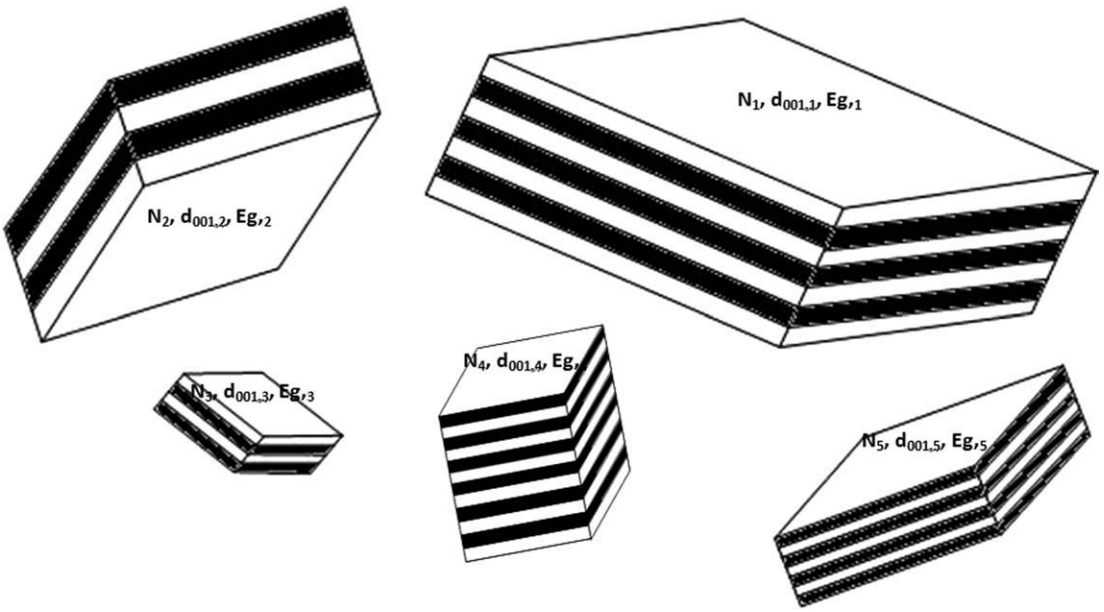

Figure 4 Schematic representation of the different morphologies of an intercalated structure (RVE) dispersed within the polymer matrix. (N_i: number of silicate layers per stack, d_i: spacing between silicate layers, E_g = modulus of the gallery phase).

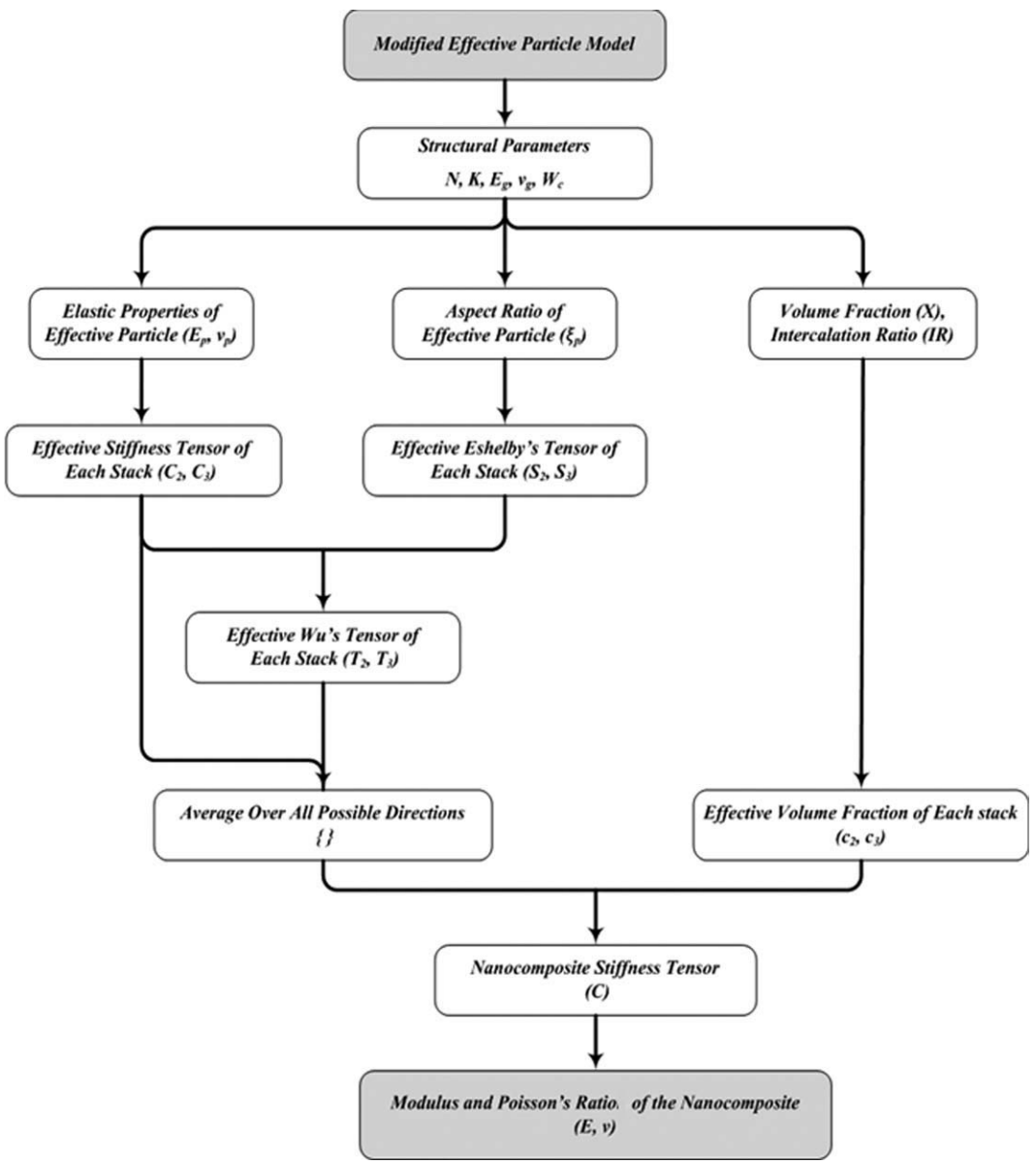

Figure 5 The sequential procedure employed here to solve the three phase form of the Mori-Tanaka equations.

$$X_N = \frac{N}{t} = \frac{N}{(N-1)d_{001} + d_s} \tag{11}$$

It can be alternatively expressed as the volume fraction of silicate in the effective particle (X):

$$X = \frac{V_c}{V_p} = \frac{Nd_s}{(N-1)d_{001} + d_s} = \frac{1}{\left[\left(1 - \frac{1}{N}\right)\left(\frac{d_{001}}{d_s}\right) + \frac{1}{N}\right]} \tag{12}$$

where V_c and V_p are the volumes assigned to the silicate sheets in a stack and the effective particle, respectively. Using eq. (10), the aspect ratio can be calculated as follows:

$$\frac{L}{t} = \frac{L}{(N-1)d_{001} + d_s} \tag{13}$$

where L is the length of the intercalated stack and shown in Figure 1. To normalize the above equations and assuming $L/d_s = 100$, eqs. (10)–(13) can be rewritten as:

$$K = \frac{d_{001}}{d_s} \tag{14}$$

$$X = \frac{N}{K(N-1) + 1} \tag{15}$$

$$\frac{L}{t} = \frac{100}{(N-1)K + 1} \tag{16}$$

Considering the multi-layer clay particle as a laminate structure with isotropic silicate sheets and orthotropic polymeric galleries, (Fig. 1), the overall elastic properties of an effective particle can be estimated as:

$$\begin{aligned} E_{p,11} &= X_N E_{\text{silicate}} d_s + (1-X) E_{\text{gallery},11} \\ &= X E_{\text{silicate}} (1-X) E_{\text{gallery},11} \end{aligned} \tag{17}$$

$$E_{p,22} = \frac{E_{\text{silicate}} E_{\text{gallery},22}}{(1 - 2\delta \nu_{\text{gallery}})[(1-X)E_{\text{silicate}} - XE_{\text{gallery},22}]} \tag{18}$$

$$\delta = \frac{E_{\text{silicate}} \nu_{\text{gallery}} - E_{\text{gallery}} \nu_{\text{silicate}}}{(1 - \nu_{\text{gallery}}) E_{\text{silicate}} (1 - \nu_{\text{gallery}}) E_{\text{gallery}}} \tag{19}$$

$$\nu_{p,12} = X\nu_{\text{silicate}} + (1-X)\nu_{\text{gallery},12} \tag{20}$$

$$G_{p,12} = \frac{G_{\text{silicate}} G_{\text{gallery},12}}{(1-X)G_{\text{silicate}} - XG_{\text{gallery},12}} \tag{21}$$

Although the elastic properties of gallery phase are not still determined, one can approximate that $E_{\text{gallery}}/E_{\text{silicate}} \ll 1$ and $G_{\text{gallery}}/G_{\text{silicate}} \ll 1$.[25] In this case, the overall $E_{p,22}$ and $G_{p,12}$ will severely decrease and thus the effect of particle anisotropy can be neglected. Therefore, only two independent elastic constants are needed to estimate the overall elastic properties of the effective particle. In this article, we approximated E_p and ν_p with $E_{p,11}$ and $\nu_{p,12}$, respectively. Consequently, the components of Eshelby and stiffness tensors of the two intercalated morphologies can be computed using eqs. (16), (17), and (19), respectively.

Another significant part of eq. (7) is the volume fraction of each phase, including c_1 (polymer matrix), c_2 (intercalated morphology 1) and c_3 (intercalated morphology 2). As it can be expected, these fractions are correlated to the structural parameters (N, d_{001} or K ratio) of the nanocomposite. First of all, the volume fraction of each phase can be defined easily as:

$$c_1 + c_2 + c_3 = 1 \tag{22}$$

$$c_1 = \frac{V_m}{V_t} \tag{23}$$

$$c_2 = \frac{V_2}{V_t} \tag{24}$$

$$c_3 = \frac{V_3}{V_t} \tag{25}$$

where V_m, V_2, V_3, and V_t are the volume of the polymer matrix, intercalated morphology 1, intercalated morphology 2, and the total volume of the nanocomposite, respectively. On the other hand, the volume of each intercalated stack (Fig. 1) can be estimated as:

$$V = V_g + V_c \tag{26}$$

$$V_g = Nd_gLt \tag{27}$$

$$V_c = Nd_sLt \tag{28}$$

where V_g, V_c, and d_g are the volume of gallery phase, clay layers, and the gallery thickness in each intercalated stack, respectively.

Alternatively, the volume of gallery phase and clay layers cane be written as:

$$V_g = \frac{w_g}{\rho_g} \tag{29}$$

$$V_c = \frac{w_c}{\rho_c} \tag{30}$$

where ρ_g and ρ_c are the gallery phase and clay densities in each intercalated stack, respectively.

Considering K ratio definition [eq. (14)] and combining eqs. (26)–(30), the volume of each intercalated stack (V_2, V_3) can be estimated as:

$$\frac{w_c}{w_g} = 4\frac{d_s}{d_g} = \frac{4}{K-1} \tag{31}$$

$$V_2 = \frac{K_2 W_{c,2}}{4} \tag{32}$$

$$V_3 = \frac{K_3 W_{c,3}}{4} \tag{33}$$

where K_2, K_3, $W_{c,2}$, and $W_{c,3}$ are the d-spacing ratio of intercalated morphology 1, feature 2, the clay weight fraction in intercalated morphology 1 and morphology 2, respectively. It should be noted that some structural parameters, including ρ_g, ρ_c, E_s, ν_s, and ρ_m, have been considered constant and are shown in Table I, based on the values reported in the literature.[14,43,44]

The weight fraction of the polymer matrix (W_m) can also be obtained as:

$$W_m = 1 - W_{c,2} - \frac{W_{c,2}(K_2-1)}{4} - W_{c,3} - \frac{W_{c,3}(K_3-1)}{4} \tag{34}$$

Combining eqs. (22) and (32)–(34), the volume fraction of each phase can be written as:

$$c_2 = \frac{K_2 W_{c,2}}{4 - W_{c,2}(3+K_2) - W_{c,3}(3+K_3)} \tag{35}$$

$$c_2 = \frac{K_3 W_{c,3}}{4 - W_{c,2}(3+K_2) - W_{c,3}(3+K_3)} \tag{36}$$

$$c_1 = 1 - c_2 - c_3 \tag{37}$$

As can be seen in eqs. (35)–(37), there are some parameters including the weight fractions of the clay layers in each intercalated morphology ($W_{c,2}$, $W_{c,3}$) which cannot be practically measured and controlled. In other words, the only practical parameter which can be controlled and measured is the total clay weight fraction ($W_{c,t}$). Therefore, it is needed to correlate $W_{c,t}$ to $W_{c,2}$, and $W_{c,3}$ by defining a new parameter called "intercalation ratio" (IR). IR is considered as the ratio of volume fraction of the intercalated morphology 1 (V_2) to the total volume fraction of intercalated structures ($V_2 + V_3$) as:

$$\mathrm{IR} = \frac{V_2}{V_2 + V_3} \tag{38}$$

Considering eqs. (32) and (33), the IR can be rewritten as:

TABLE I
The Constant Parameters Considered in the Micromechanical Model[14,42,43]

Parameter	Definition	Value
ρ_m	Density of the polymeric matrix	$\approx$1 g/cm^3
ρ_g	Density of the gallery phase	$\approx$1 g/cm^3
ρ_c	Density of the clay layers	$\approx$4 g/cm^3
E_s	Modulus of the silicate sheets	$\approx$400 GPa
ν_s	Poisson's ratio of the silicate sheets	$\approx$0.2

$$\mathrm{IR} = \frac{K_2 W_{c,2}}{K_2 W_{c,2} + K_3 W_{c,3}} \tag{39}$$

Accordingly, the weight fraction of clay layers in each intercalated morphology ($W_{c,2}$, $W_{c,3}$) can be computed versus total clay weight fraction ($W_{c,t}$) as:

$$\frac{w_{c,2}}{w_{c,1}} = \frac{K_3}{K_2(1-IR)} \equiv \alpha \tag{40}$$

$$W_{c,t} = W_{c,2} - W_{c,3} \tag{41}$$

$$W_{c,2} = \frac{\alpha}{1+\alpha} W_{c,t} \tag{42}$$

$$W_{c,3} = \frac{1}{1+\alpha} W_{c,t} \tag{43}$$

Consequently, through the above equations the clay weight fraction in each intercalated morphology ($W_{c,2}$, $W_{c,3}$), which are not practically measurable, have been calculated based upon the well-known processing parameters. These parameters include total clay weight fraction ($W_{c,t}$) and d-spacing between the silicate layers in each intercalated morphology (K_2, K_3). It should be noted that K and N parameters associated with each feature can be estimated from X-ray diffraction analysis (XRD) and TEM images, respectively.[17,36,44] In addition, IR of each fully intercalated specimen can be approximated using TEM images by either quantitative analysis or visual identification. Combining eqs. (40)–(43) with eqs. (35)–(37), the volume fraction of each phase (c_1,c_2,c_3) are calculated based on the parameters which can be experimentally measured. These parameters are the number of silicate layers per stack (N), the d-spacing between the layers (K), IR and the total clay weight fraction ($W_{c,t}$).

In addition to the Eshelby's and stiffness tensors and volume fraction of each phase, the last part of eq. (7) is averaging over all possible orientations {} of the intercalated stacks [eqs. (3)–(5)]. Although researchers such as Schjodt and Pyrz[22,45] have proposed some orientation distribution functions for conventional composites, there seems not to be applied on PLSNs with hierarchical structures. In

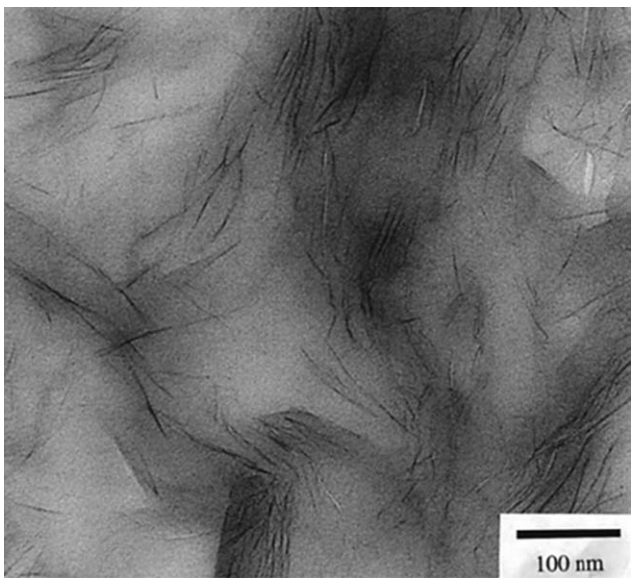

Figure 6 TEM image of 10 wt % Cloisite 30A in a diamine-cured epoxy representing random distribution of the both clay platelets and clay intercalated stacks.[46]

other words, it is difficult to define a specific distribution function for different structural scales in vicinity of each other. On the other hand, many TEM images such as that shown in Figure 6[46] illustrate approximately a random distribution of both clay stacks (intercalated structures) and individual platelets (exfoliated structure) within the polymer matrix. Therefore, the orientation distribution function (f) in eq. (5) would take a constant value ($1/8\pi^2$) and would not take part in the integral[47] as follows:

$$\{C\} = 1/8\pi^2 \int_0^{2\pi}\int_0^{2\pi}\int_0^{\pi} C_{ijkl}(\theta,\varphi,\psi) \times \sin(\theta) d\theta d\varphi d\psi \quad (44)$$

As seen, all the elements of eqs. (7)–(9) have been calculated and a thorough multi-scale micromechanical model has been developed which considers most of the affecting parameters, including gallery phase modulus (E_g), IR, silicate layers spacing (d_{001} or K ratio), number of the silicate layers per stack (N), aspect ratio of the intercalated stack (L/t), matrix modulus (E_m) and the total clay weight fraction ($W_{c,t}$). The influences of these parameters on Young's modulus of PLSNs containing two distinguished intercalated morphologies have been investigated next in the following sections.

Numerical results and discussion

Here, by employing the new micromechanical approach proposed in Model development section, the structural influences (N, d_{001}, IR, E_g) on Young's modulus of epoxy-clay nanocomposites containing two intercalated morphologies have been calculated as a function of total clay weight fraction ($W_{c,t}$). Because the aspect ratio (L/t) of each intercalated stack depends strongly on d-spacing between silicate layers (d_{001}) and number of silicate layers (N), it cannot be analyzed independently. The cumulative effects of N and d_{001} on the aspect ratio of each stack (L/t) have been discussed in details next in Spacing between the silicate layers section.

Number of silicate layers per stack (N)

Assuming two distinguished intercalated morphologies exist, the effect of N_2 (number of silicate layers in feature 2) on Young's modulus of a typical epoxy-clay nanocomposite is investigated and shown in Figure 7. For simplicity, the number of silicate layers per stack of feature 1 (N_1) and the other parameters have been considered constant and are illustrated on the top of the figure. As experimentally expected, by increasing N_2 ($\geq$1), the nanocomposite's modulus drastically decreases. This is due to the fact that at high values of N, the individual clay platelets touch each other's and compose the intercalated stacks.

Spacing between the silicate layers (d_{001})

The d-spacing between the silicate layers in each intercalated stack (d_{001} or K ratio) is the other structural parameter which strongly affects Young's modulus of PLSNs. Figure 8 illustrates the K ratio effect of feature 2 (K_2) on the modulus of epoxy-clay nanocomposite containing two different intercalated morphologies. Comparing Figures 7 and 8 reveals that d_{001} (K ratio) is much more influential on the modulus than N, as experimentally reported by the

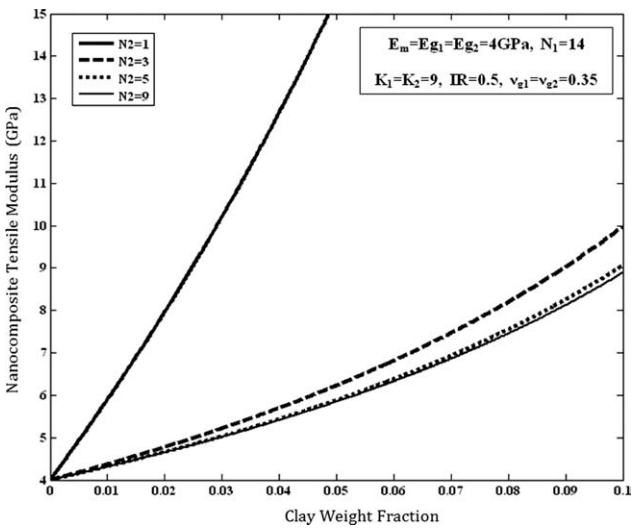

Figure 7 The influence of N_2 on Young's modulus of epoxy-clay nanocomposite.

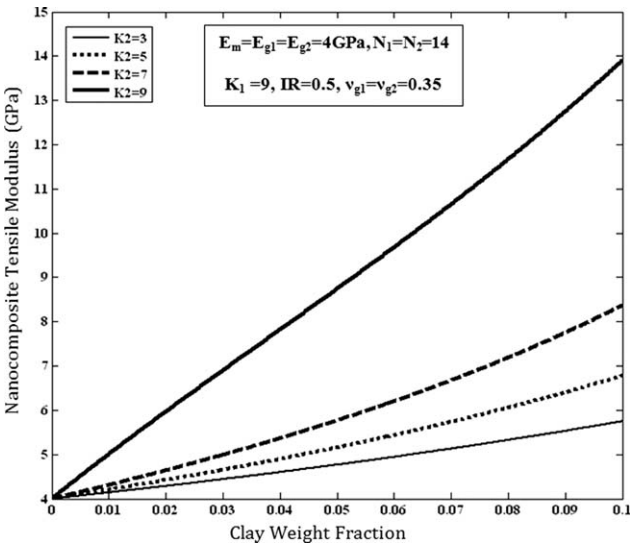

Figure 8 The effect of K_2 on Young's modulus of epoxy-clay nanocomposite.

researchers.[48,49] This important result has not been considered through the previous models.[18,24,25]

Although the number of silicate layers (N) and d-spacing between them in each stack can individually affect the nanocomposite's modulus, it is necessary to consider the cumulative influences of these parameters when some of the intercalated stacks have been broken into small ones. Under these circumstances, as shown schematically in Figure 9, two different possibilities can be supposed including increase in aspect ratio (L/t) by decreasing K ratio and keep in constant by increasing K ratio. In both cases, the number of silicate layers per stack (N) decrease, but at the same silicate layer thickness (d_s). Therefore, in the first case, aspect ratio is the dominant parameter while in the second case K ratio is the dominant factor.

Modulus of the gallery phase (E_g)

Although the previous researchers[18,24,25] neglected the gallery phase properties, recent experimental results such as those reported in Ref. 33 highlight the importance of the gallery phase on overall properties of the PLSNs. Illustrating the contribution of the gallery phase modulus (E_g) on Young's modulus of PLSNs is the first outstanding attribute of the current micromechanical approach proposed in this article. Figure 10 illustrates the influence of E_{g2} (feature 2) on the modulus of epoxy-clay nanocomposite containing two different intercalated morphologies in which the constant parameters are shown on the figure.

Based on the mechanism called the kink model of melt intercalation, this is quite reasonable that the polymer chains in the gallery have different conformations from those of the molecules in the bulk of the matrix. The constraint applied on the polymer chains within the gallery which results in a more rigid behavior compared with the bulk of the matrix has been claimed.[50] However, some researchers have argued a more flexible behavior for the gallery phase due to the plasticizing effect of the clay surfactants.[33] These two scenarios are schematically illustrated in Figure 11. Therefore, there is a direct relationship between K ratio and E_g in which both of them drastically increase the nanocomposite's modulus, as shown in Figures 8 and 10. However, seems there is an optimal interlayer spacing (Fig. 11) in which minimizes unfavorable interactions between the polymer chain and the silicate layers. In this case, sufficient shear force causes a kink to form in the clay sheet as a form of compression failure. Polymer can then penetrate the new space between the layers and kink can propagate along the layer, and more polymer chains can intercalate. This mechanism can explain the large stiffness of the gallery phase between the silicate layers.[50] In other words, after the optimum point the gallery phase modulus does

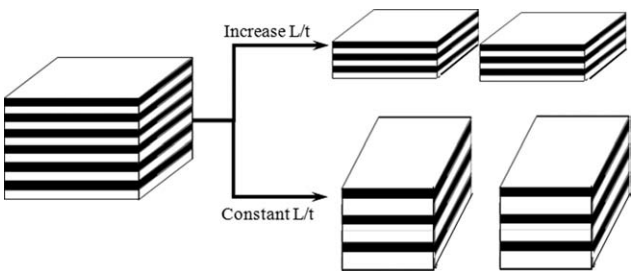

Figure 9 Schematic representation of breaking an intercalated stack into small ones illustrating cumulative effects of K ratio and N.

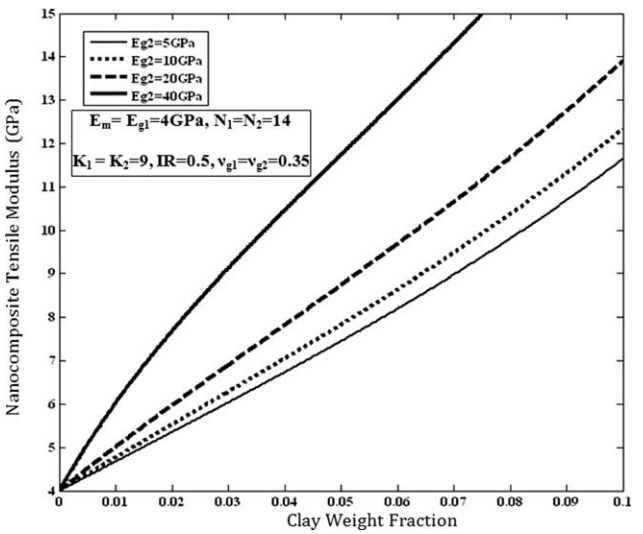

Figure 10 The effect of E_{g2} on Young's modulus of epoxy-clay nanocomposite.

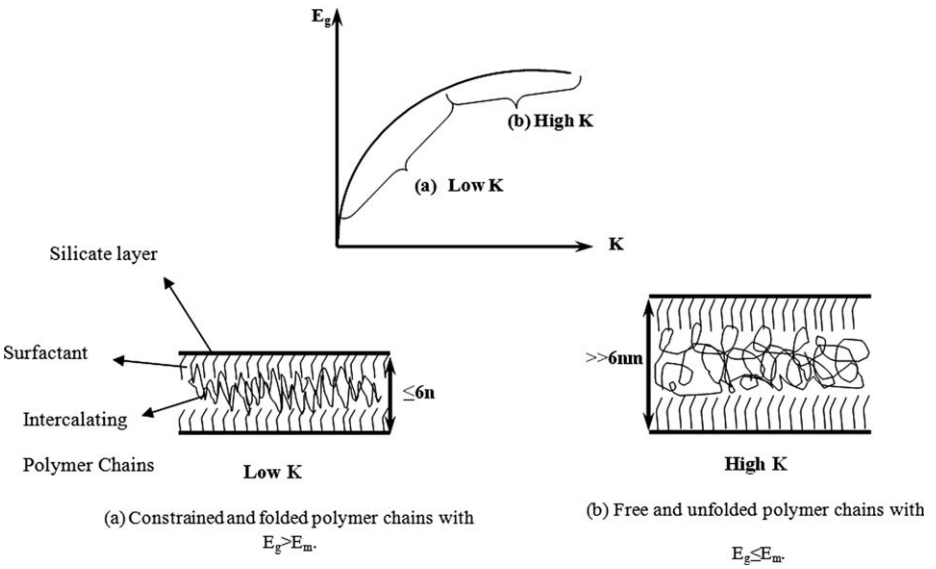

Figure 11 Schematic illustration the effect of K variations on the gallery phase modulus (E_g).

not significantly change when K ratio increases. Some researchers[33,50] reported that the optimum d_{001} is about 6 nm which strongly affected gallery phase modulus (E_g) and finally the nanocomposite's modulus. Based on the molecular characterization conducted by Manevitch and Rutledge,[43] the silicate sheet thickness (d_s) can be assumed about 0.6 nm and correspondingly, the optimum K ratio would be about 10.

Intercalation ratio

In addition of gallery phase modulus (E_g), considering two different intercalated morphologies in vicinity of each other's, which have been defined using IR [eq. (39)], is the second outstanding attributes of the new micromechanical model proposed in this article. In fact, IR demonstrates the concurrent effects of nanostructural parameters (N, K, E_g) which can be estimated using TEM images. According to the results achieved in previous sections, the nanocomposite's modulus increases when N decreases and K and E_g increases, respectively. Therefore, it can be expected that by increasing the volume fraction of those intercalated morphologies, which are attributed to large K and E_g and small N, Young's modulus of PLSNs would have been increased. This important result is quantitatively illustrated in Figure 12 for epoxy-clay nanocomposite using IR definition.

Experimental verifications

To evaluate the multi-scale micromechanical model, the results of the model have been compared with both the previous model proposed by the authors[34] and some of the experimental data obtained in the

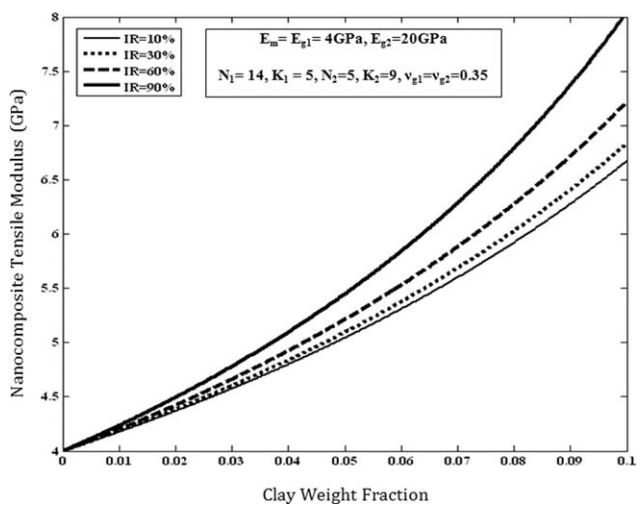

Figure 12 Micromechanical modeling results representing IR effect on Young's modulus of epoxy-nanocomposite.

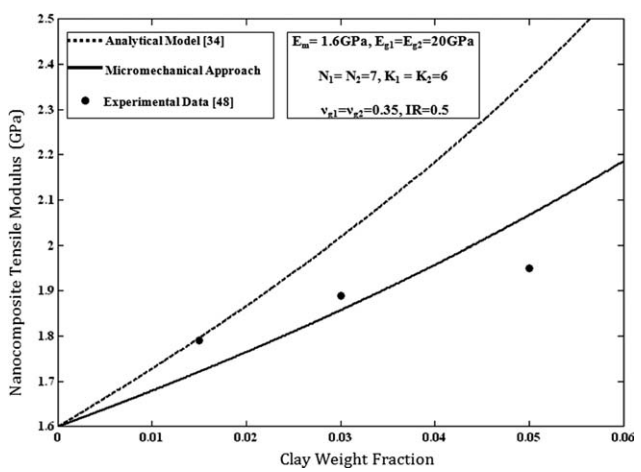

Figure 13 Micromechanical modeling results in comparison with the experimental data for PP/clay nanocomposite.[48]

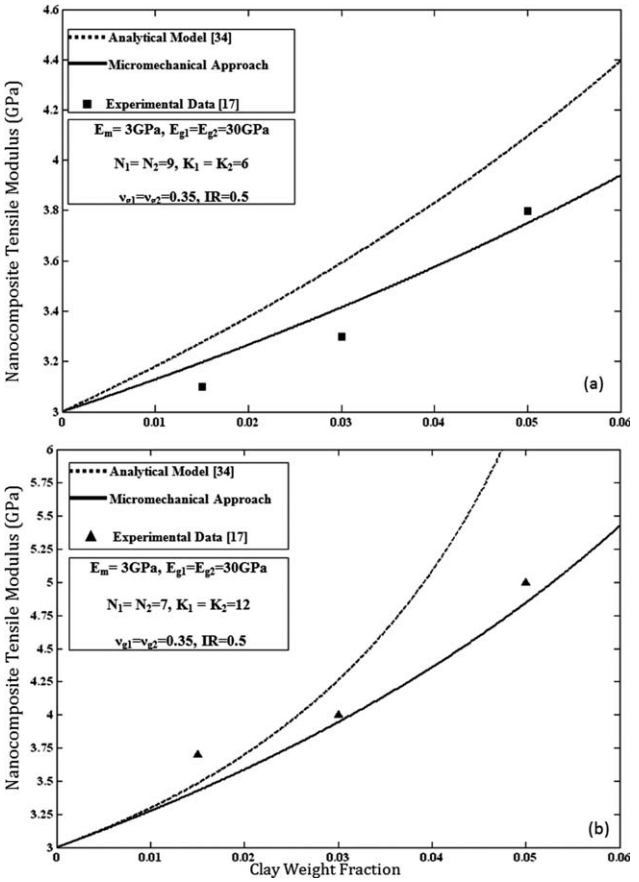

Figure 14 Micromechanical modeling results in comparison with the experimental data representing the effect of K ratio variations on the modulus of (a) Epoxy/DK1 and (b) Epoxy/I.30E nanocomposites.[17]

same group for epoxy/clay[17] and PP/clay[48] nanocomposites.

Figure 13 illustrates the micromechanical results together with the previous model[34] and experimental data for PP/clay[48] nanocomposite. The micromechanical results based on the Mori-Tanaka model shows better agreement with the experimental data than the previous analytical model,[34] however, none of the models could match the trend of the experimental data. According to Li et al.,[51] this discrepancy can be attributed to the possible agglomeration of silicate layers at higher clay loadings which results in lower modulus enhancement than that expected.

Marouf et al.[17] used two different types of clay i.e., DK1 (from FCC) and I.30E (from Nanocor) in an epoxy matrix to investigate the effect of *d*-spacing between the silicate layers in the intercalated structures. They have shown that increase in *d*-spacing between the silicate layers in an intercalated stack results in increasing the nanocomposite's modulus. This important result is well predicted by the new micromechanical model and is compared with the previous analytical model together with the experimental data, as shown in Figure 14(a) and (b). It can be seen that the micromechanical results are again in better agreement with the experimental data than the analytical approach proposed by the authors in their previous work.[34]

It should be noted that *d*-spacing between the silicate layers (K) and number of silicate layers per stack (N) used in the micromechanical model are estimated from XRD and TEM images, respectively, as reported in the above experimental works.[17,43]

CONCLUSION

In this article, a new multi-scale micromechanical approach based on the Mori-Tanaka model combined with the effective particle concept has been proposed considering the most important nanostructural characteristics of PLSNs containing different intercalated morphologies. These characteristics include the aspect ratio of both individual clay platelet and intercalated stack, the number of silicate layers per stack, *d*-spacing between the layers, modulus of the gallery phase, and IR. It is shown that the simultaneous effects of *d*-spacing between the silicate layers and gallery phase modulus remarkably change the nanocomposite's modulus, compared with the effect of the number of silicate layers per stack. In addition, it is found that there is an optimum point for *d*-spacing to increase the nanocomposite's modulus which is estimated about 6 nm. In other words, after the optimum point the gallery phase modulus does not significantly change when *d*-spacing increases. Comparing the micromechanical modeling results with the experimental data illustrates the new approach is more accurate than the previous model developed by the same authors.

NOMENCLATURE

m_ν	Matrix Poisson's ratio
$\nu_{gallery}$	Gallery Poisson's ratio
$\nu_{silicate}$	Silicate Poisson's ratio
d_{001}	Spacing between the silicate layer
d_s	Silicate layer thickness
d_g	Gallery phase thickness
K	*D*-spacing ratio (d_{001}/d_s)
K_2	*D*-spacing ratio of intercalated phase 1
K_3	*D*-spacing ratio of intercalated phase 2
S	Eshelby's tensor
S_2	Eshelby's tensor of intercalated phase 1
I	Fourth-order symmetric unit tensor
E	Nanocomposite's modulus
θ,ψ,ϕ	Euler's angles
$f(\theta,\Psi,\phi)$	Orientation distribution function
V_c	Volume of silicate layers per stack

V_p	Volume of an intercalated stack
V_t	Total volume of the nanocomposite
V_g	Volume of gallery phase per stack
V_1	Volume of polymer matrix
V_2	Volume of intercalated phase 1
V_3	Volume of intercalated phase 2
G_{silicate}	Shear modulus of the silicate layer
G_{gallery}	Shear modulus of the gallery pha
ρ_m	Density of the polymer matrix
C	Nanocomposite's stiffness tensor
C_1	Matrix stiffness tensor
C_2	Stiffness tensor of intercalated phase 1
C_3	Stiffness tensor of intercalated phase 2
T	Matrix Wu's tensor
T_2	Wu's tensor of intercalated phase 1
T_3	Wu's tensor of intercalated phase 2
c_1	Matrix volume fraction
c_2	Volume fraction of intercalated phase 1
c_3	Volume fraction of intercalated phase 2
X	Volume fraction of silicate in the effective particle
X_N	Number of silicate sheets per unit particle thickness
t	Thickness of an intercalated stack
N	Number of silicate layers per stack
W_m	Weight fraction of polymer matrix
W_g	Weight fraction of gallery phase per stack
W_c	Weight fraction of silicate layers per stack
$W_{c,2}$	Weight fraction of silicate layers in intercalated phase 1
$W_{c,3}$	Weight fraction of silicate layers in intercalated phase 2
$W_{c,t}$	Total clay weight fraction
IR	Intercalation ratio
$E_{p,11}$	Longitudinal modulus of the effective particle
E_{silicate}	Modulus of the silicate layers
E_{gallery}	Modulus of the gallery phase
ρ_c	Density of the clay silicate layers
ρ_g	Density of the gallery phase

APPENDIX: COMPONENTS OF ESHELBY'S TENSOR (S_{IJKL})

The components of the Eshelby's tensor for a three dimensional ellipsoidal inclusion with no axes of symmetry [Fig. 1(a)] can be found in the book of Mura.[41] In the case of clay stacks, because $a_1 = a_3 \gg a_2$, the equations can be simplified and are shown below as a function of clay stack aspect ratio ($A = a_1/a_2$)

$$S_{1111} = S_{2222} = \frac{(13 - 8\nu)\pi}{32(1-\nu)A}$$

$$S_{1122} = S_{2211} = \frac{(8\nu - 1)\pi}{32(1-\nu)A}$$

$$S_{1133} = S_{2233} = \frac{(2\nu - 1)\pi}{8(1-\nu)A}$$

$$S_{1212} = \frac{(7 - 8\nu)\pi}{32(1-\nu)A}$$

$$S_{2323} = S_{3131} = 0.5\left[\frac{(\nu - 2)\pi}{4(1-\nu)A} + 1\right]$$

$$S_{3322} = S_{3311} = \frac{\nu}{1-\nu}\left[1 - \frac{(4\nu - 1)\pi}{8\nu A}\right]$$

$$S_{3333} = 1 - \frac{(1 - 2\nu)\pi}{4(1-\nu)A}$$

References

1. Liu, T. X.; Liu, Z. H.; Ma, K. X.; Shen, L.; Zeng, K. Y.; He, C. B. Compos Sci Technol 2003, 63, 331.
2. Powell, C. E.; Beall, G. W. Curr Opin Solid State Mater Sci 2006, 10, 73.
3. Yoon, P. J.; Fornes, T. D.; Paul, D. R. Polymer 2002, 43, 6727.
4. Gilman, J. W. Appl Clay Sci 1999, 15, 31.
5. Messersmith, P. B.; Giannelis, E. P. Chem Mater 1994, 6, 1719.
6. Messersmith, P. B.; Giannelis, E. P. J Polym Sci Polym Chem 1995, 33, 1047.
7. Ganter, M.; Gronski, W.; Semke, H.; Zilg, T.; Thomann, R.; Muhlhaupt, R. Kautsch Gummi Kunst 2001, 54, 166.
8. Ke, Y. C.; Stroeve, P. In: Polymer Layered Silicate and Silica Nanocomposites; 1st ed. Elsevier BV: Amsterdam, The Netherlands, 2005, Chapter 1, p 62.
9. Okada, A.; Usuki, A. Macromol Mater Eng 2006, 291, 1449.
10. Bharadwaj, R. K.; Mehrabi, A. R.; Hamilton, C.; Trujillo, C.; Murga, M.; Fan, R.; Chavira, A.; Thompson, A. K. Polymer 2002, 43, 3699.
11. Ding, C.; Jia, D.; He, H.; Guo, B.; Hong, H. Polym Test 2005, 24, 94.
12. Usuki, A.; Tukigas, A.; Kato, M. Polymer 2002, 43, 2185.
13. Li, P.; Song, G.; Yin, L.; Sun, C.; Wang, L. Iran Polym J 2007, 16, 16.
14. Wu, Y. P.; Jia, Q. X.; Yu, D. S.; Zhang, L. Q. Polym Test 2004, 23, 903.
15. Nam, P. H.; Maiti, P.; Okamoto, M.; Kotaka, T.; Hasegawa, N.; Usuki, A. Polymer 2001, 42, 9633.
16. Osman, M. A.; Rupp, I. E. P.; Suter, U. W. Polymer 2005, 46, 1653.
17. Marouf, B. T.; Bagheri, R.; Pearson, R. A. Int J Mod Phys B 2008, 22, 3247.
18. Brune, D. A.; Bicerano, J. Polymer 2002, 43, 369.
19. Hocine, N. A.; Mederic, P.; Aubry, T. Polym Test 2008, 27, 330.
20. Hbaieb, K.; Wang, Q. X.; Chia, Y. H. J.; Cotterell, B. Polymer 2007, 48, 901.
21. Figiel, L.; Buckly, C. P. Comput Mater Sci 2009, 44, 1332.
22. Schjodt, J. T.; Pyrz, R. Mech Mater 2000, 32, 349.
23. Wang, J.; Pyrz, R. Compos Sci Technol 2004, 64, 925.
24. Luo, J. J.; Daniel, I. M. Compos Sci Technol 2003, 63, 1607.
25. Sheng, N.; Boyce, M. C.; Parks, D. M.; Rutledge, G. C.; Abes, J. I.; Cohen, R. E. Polymer 2004, 45, 487.
26. Lee, K. Y.; Paul, D. R. Polymer 2005, 46, 9064.
27. Choonghee, J. O.; Jin, F. U.; Naguib, H. E. Polym Eng Sci 2006, 46, 1787.
28. Cho, J.; Luo, J. J.; Daniel, I. M. Compos Sci Technol 2007, 67, 2399.

29. Jiang, B.; Liu, C.; Zhang, C.; Wang, B.; Wang, Z. Compos B 2007, 38, 24.
30. Sejnoha, M.; Zeman, J. Int J Eng Sci 2008, 46, 513.
31. Mori, T.; Tanaka, K. Acta Metall Mater 1973, 21, 571.
32. Tucker, C. L.; Liang, E. Compos Sci Technol 1999, 59, 655.
33. Adame, D.; Beall, G. W. Appl Clay Sci 2009, 42, 545.
34. Yazdi, A. Z.; Bagheri, R.; Kazeminezhad, M. J Compos Mater 2009, 43, 2921.
35. Chen, T.; Dvorak, G. J.; Benveniste, Y. J Appl Mech 1992, 59, 539.
36. Benveniste, Y. Mech Mater 1987, 6, 147.
37. Wu, T. T. Int J Solids Struct 1966, 2, 1.
38. Eshelby, J. D. Proc R Soc Lond 1957, A241, 376.
39. Mura, T. Micromechanics of Defects in Solids, 2nd ed; Martinus Nijhoff: The Hague, 1987, pp 74.
40. Manevitch, O. L.; Rutledge, G. C. J Phys Chem B 2004, 108, 1428.
41. Weon, J. I.; Sue, H. I. Polymer 2005, 46, 6325.
42. Marouf, B. T.; Pearson, R. A.; Bagheri, R. Mater Sci Eng A 2009, 515, 49.
43. Schjodt, T.; Pyrz, R. Mech Mater 2001, 33, 531.
44. Brown, J. M.; Curliss, D.; Vaia, R. A. Chem Mater 2000, 12, 3376.
45. Huang, J. H. Compos A 2001, 32, 1573.
46. Akbari, B.; Bagheri, R. J Appl Polym Sci 2009, 114, 3751.
47. Akbari, B.; Bagheri, R. Eur Polym J 2007, 43, 782.
48. Ajayan, P. M.; Schadler, L. S.; Braun, P. V. In: Nanocomposites Science and Technology; Schadler, L. S., Ed.; Weinheim: Wiley-Vch, 2003, Chapter 2; pp 103–111.
49. Li, P.; Song, G.; Yin, L.; Sun, C.; Wang, L. Iran Polym J 2007, 16, 775.
50. Alexandre, M.; Dubois, P. Mater Sci Eng 2000, 28, 1.
51. Nemat-Nasser, S.; Hori, M. Micromechanics: Overall Properties of Heterogeneous Materials. In: North-Holland Series in Applied Mathematics and Mechanics; North-Holland, Amsterdam, 1993.